Earth and Planetary Science Letters 487 (2018) 127–137

Contents lists available at ScienceDirect

Earth and Planetary Science Letters

www.elsevier.com/locate/epsl

Salt precipitation and dissolution in the late Quaternary Dead Sea: Evidence from chemical and δ^{37}Cl composition of pore fluids and halites

Elan J. Levy [a,b,*], Yoseph Yechieli [b,c], Ittai Gavrieli [b], Boaz Lazar [d], Yael Kiro [e], Mordechai Stein [b,d], Orit Sivan [a]

[a] Department of Geological and Environmental Sciences, Ben-Gurion University of the Negev, Beer Sheva, Israel
[b] Geological Survey of Israel, 30 Malkhe Israel St., Jerusalem, 95501, Israel
[c] Department of Hydrology and Microbiology, Zuckerberg Center, Ben-Gurion University of the Negev, Sede Boker, Israel
[d] Institute of Earth Sciences, The Hebrew University, Givat Ram, Jerusalem, 91904, Israel
[e] Lamont-Doherty Earth Observatory, 61 Route 9W, PO Box 1000, Palisades, NY 10964, United States

ARTICLE INFO

Article history:
Received 2 November 2017
Received in revised form 18 January 2018
Accepted 2 February 2018
Available online 12 February 2018
Editor: M. Frank

Keywords:
Dead Sea
halite dissolution
halite precipitation
δ^{37}Cl
Mount Sedom salt diapir
ICDP

ABSTRACT

The chemical composition and δ^{37}Cl of pore fluids from the ICDP core drilled in the deepest floor of the terminal and hypersaline Dead Sea, and halites from the adjacent Mount Sedom salt diapir, are used to establish the dynamics of halite precipitation and dissolution during the last interglacial and glacial periods. Between ~132 and 116 thousand years ago (ka) halites precipitated in the lake resulting in the expulsion of Na^+ and Cl^- from the residual solution. Over 50% of the Cl^- reservoir was removed, resulting in a decrease in the Na/Cl ratio from 0.57 to 0.19. This process was accompanied by a decrease in δ^{37}Cl values in the precipitating halites and the associated residual Cl^- in the lake. The observed decrease fits a Rayleigh distillation curve with a fractionation factor of $\Delta_{(NaCl\text{–}Dead\ Sea\ solution)} = +0.32‰$ (±0.12) determined in the present study. This behavior implies negligible contribution of external sources of Cl^- to the lake during the main peak of the last interglacial, MIS5e. Subsequently, during the last glacial (ca. 117 to 17 ka) dissolution of halite took place, the Na^+ and Cl^- inventory were replenished, accompanied by an increase in Na/Cl from 0.21 to 0.55 and in the δ^{37}Cl values from −0.46‰ to −0.12‰. While the lake underwent significant dilution during that time, the decrease in salinity was somewhat suppressed by the dissolution of the halite which was mostly derived from Mount Sedom salt diapir.

1. Introduction

Salt deposits are often found in geological records from marine settings, such as sediments pertaining to the Messinian Salinity Crisis (MSC), and sedimentary sections from closed terminal hypersaline lakes, such as the Great Salt Lake. Of these, halite is a common evaporite mineral that may accumulate to thickness of several km's (e.g. the MSC salt deposits; Hsü et al., 1973). Reconstruction of the paleo-environmental conditions and chemical composition of the halite deposits and its precipitating solutions can be done by evaluation of the chemical and isotope composition (e.g. ^{37}Cl) of the crystals and their associated fluid inclusions, along with accompanying pore fluids (e.g. Eggenkamp et al., 1995; García-Veigas et al., 2009; Kiro et al., 2017; Levy et al., 2017).

Situated at the lowest accessible point on earth at ~432 m below mean sea level (year 2017), the Dead Sea is currently one of the most concentrated natural water bodies with a salinity of ~28%. Its negative water balance over the past decades has resulted in continuous lake level decline and halite precipitation (Steinhorn, 1983; Gavrieli et al., 1989; Gavrieli, 1997; Lensky et al., 2005; Sirota et al., 2017). The unique Ca-chloride composition of the brine comprising the Dead Sea solution began its evolution during the Miocene with the penetration of evaporated seawater into the tectonic depressions of the Kinnarot and Dead Sea basins. Further evaporation in the "Sedom Lagoon" resulted in the accumulation of a thick salt deposit that today is exposed at the Mount Sedom salt diapir to the south west of the Dead Sea (Zak, 1967; Fig. 1). Interaction of the solution with the surrounding Cretaceous limestone rocks further modified its composition, depleting it of bicarbonate and sulfate. The resulting Ca-chloride brine is

* Corresponding author at: Department of Geological and Environmental Sciences, Ben-Gurion University of the Negev, Beer Sheva, Israel.
E-mail address: elanl@post.bgu.ac.il (E.J. Levy).

https://doi.org/10.1016/j.epsl.2018.02.003
0012-821X/

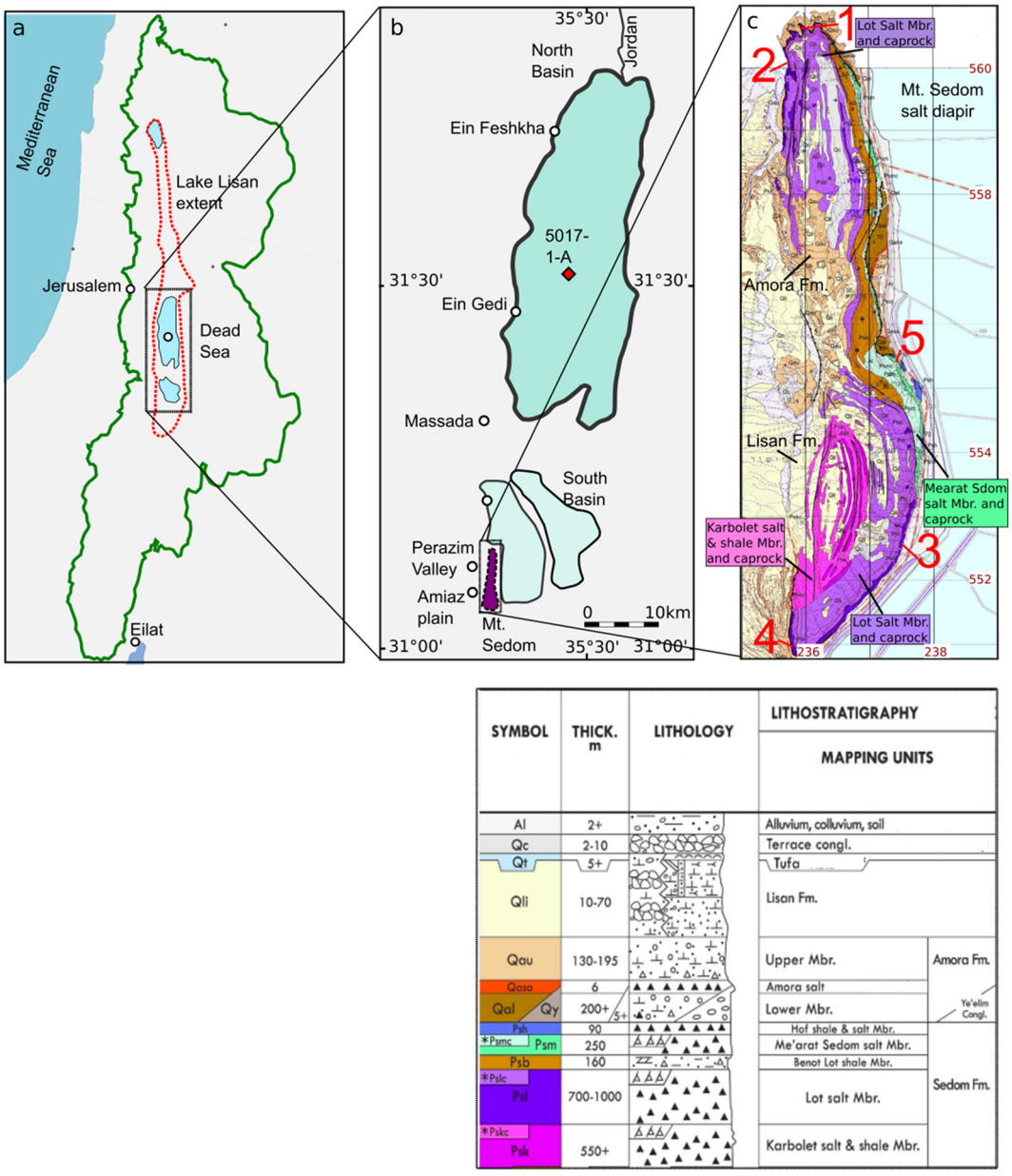

Fig. 1. Regional Setting. (a) Map of Dead Sea, watershed (green line), and Last Glacial Dead Sea (Lake Lisan) maximum extent (red dotted line); (b) Location of core 5017-1-A (red diamond) and Mt. Sedom salt diapir (purple); (c) Geological map of the Mt. Sedom including its five members, respective caprock members, and sediments (e.g. Lisan Fm., Amora Fm.) (adapted from Agnon et al., 2006; Zak, 1967). The lithological legend is shown to the bottom. Salt samples retrieved from Lot Salt Mbr numbered #1–4 and the sample from Mearat Sedom Mbr. is located at #5 (red). Geographical coordinate system used is Israel Transverse Mercator (ITM). (For interpretation of the references to color in this figure legend, the reader is referred to the web version of this article.)

characterized by $Na/Cl < 1$ and $Ca/(HCO_3 + SO_4) > 1$, composition that dictates the modes of primary minerals formation in the lakes that has since occupied the Dead Sea depression, i.e., mostly formation of primary aragonite or gypsum (Starinsky, 1974; Stein, 2014). Halite deposits can also be found in the sedimentary outcrops and drilled cores of the Dead Sea and precursor terminal water bodies of the region that evolved throughout the Pleistocene.

Over the late Quaternary the compositions of the hypersaline lakes filling the Dead Sea Basin varied significantly reflected the hydrological-climate conditions in the lake's large watershed (Stein, 2014). The alternating lake deposits comprising of authigenic evaporite deposits interbedded in the lacustrine sequences with clastic sediments provide high resolution sedimentary records that were extensively used for regional paleo-climate reconstruction (Stein, 2001, 2014; Stein et al., 2010; Torfstein et al., 2015; Palchan et al., 2017). While most of these studies were done at the exposed marginal terraces of the modern Dead Sea, information from the depocenter of the lake was gathered only following the drilling of cores at the deep floor of the Dead Sea in 2010–2011, the Dead Sea Deep Drilling Project (DSDDP) performed under the umbrella of the International Continental Drilling Project (ICDP) (Stein et al., 2011; Neugebauer et al., 2014). The drilling recovered a 456 m long sediment core (Core 5017-1-A) from 300 m below lake level (m bll) and provided for the first time a high-resolution sedimentary record of the deep lake spanning ca. 220 ka (Neugebauer et al., 2014, 2016; Torfstein et al., 2015) (Fig. 1a and 1b).

The pore fluids extracted from the detrital sediments were used as proxies for compositional changes of the deep lake over time. The $\delta^{18}O$ and Cl^- of the pore fluids were used to reconstruct the salinity in the deep lake of the last glacial Dead Sea (Lazar et al., 2014), which became diluted as a result of mixing with less saline

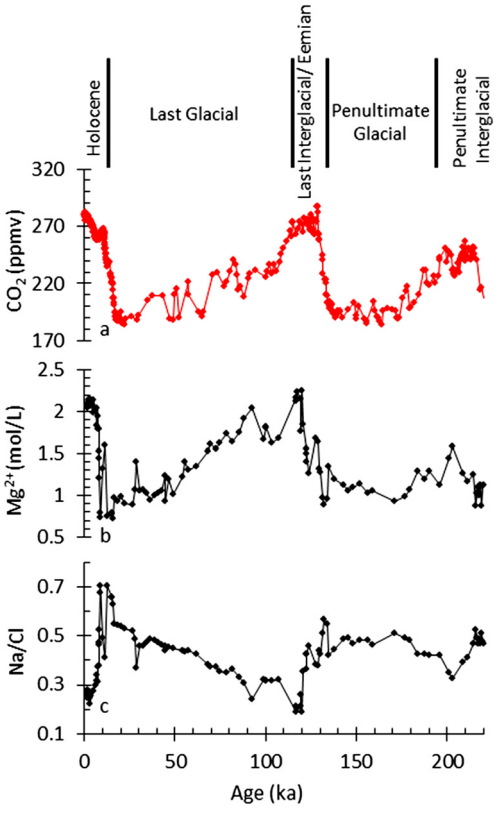

Fig. 2. Pore fluid chemistry from core 5017-1-A and correlation to global climate change as emphasized by: (a) CO_2 record from Antarctic ice cores (Lüthi et al., 2008); (b) Brine concentration and dilution, expressed by Mg^{2+} concentrations; (c) Change in Na/Cl ratio controlled by halite precipitation and dissolution.

waters. Moreover, the conservative Br^- and Mg^{2+} concentrations varied in the lake as a response to the hydrological conditions in the lake's watershed, concentrating when the lake shrinked and diluting when the lake expanded (Levy et al., 2017).

The Na/Cl ratio also showed variability in the pore fluids. The variations in the conservative Br^- and Mg^{2+} and non-conservative Na/Cl reflected changes in the lake volume and chemistry as a result of long-term regional climate changes, with a characteristic cyclic glacial–interglacial pattern as observed in global climate records such as atmospheric CO_2 from Antarctic ice cores (Fig. 2; Lüthi et al., 2008; Levy et al., 2017). During interglacial periods, when lake volume decreased and conservative ion concentrations increased, the Na/Cl ratio in the pore fluids and halite fluid inclusions decreased (Levy et al., 2017; Kiro et al., 2017). Given the brine's Na/Cl < 1, a decrease in the ratio implies that halite precipitation took place as Na^+ and Cl^- would be removed at a ratio of 1:1. Conversely, during periods of lake expansion and decreasing conservative ion concentrations, such as the last glacial period, the Na/Cl ratios in the pore-fluids increased, suggesting that both Na^+ and Cl^- were added to the lake brine as a result of halite dissolution.

The fractionation of stable isotope of chlorine (expressed in the $\delta^{37}Cl$ notation) during halite precipitation allows the evaluation of halite precipitation and dissolution processes and their reconstruction from the geological record (Eggenkamp et al., 1995; Stiller et al., 1998; García-Veigas et al., 2009; Luo et al., 2012). Stiller et al. (1998) investigated the hydrological and limnological system of the modern Dead Sea from a ^{37}Cl standpoint. Additionally, geochemical and isotope analyses, including $\delta^{37}Cl$, of the evaporite sequence of the Mount Sedom salt diapir indicate that evaporation of seawater and mixture of seawater and continental water played a role in the formation of these salts (García-Veigas et al., 2009).

Here, we focus on the process of halite precipitation and dissolution in the hypersaline Dead Sea brine during the last interglacial and glacial time intervals (ca. 132–14 ka). We combine chemical and $\delta^{37}Cl$ isotope data from pore fluids and halite samples that were recovered from the DSDDP core and sampled from the exposures of the Mount Sedom salt diapir. Mass balance calculations along with geological observations allow the quantification of halite dissolution and its effect on the lake chemistry during the last glacial period. Finally we show that the Mount Sedom salt diapir was a major source of the halite that dissolved and supplied the Na^+ and Cl^- to the lake, and as such was able to counteract the effects of lake level rise and increasing volume on the solution and maintain high salinity.

2. The Mount Sedom salt diapir

Mount Sedom is located at the south west of the modern Dead Sea and is built of sequences of halite, anhydrite and some dolomite that comprise the late Miocene Sedom Formation. The Sedom Formation is overlaid by sequences of lacustrine sediments comprising the Pleistocene Amora, Samra and Lisan Formations (Zak, 1967; Stein, 2014). The age of the Sedom Formation was estimated by ^{10}Be atmospheric dating of the salt units and $^{10}Be/^{26}Al$ burial dating to lie between 3–6 Ma (Belmaker et al., 2013; Matmon et al., 2014). The diapir intruded the overlying Quaternary lacustrine sequences uplifted and tilted them (Weinberger et al., 2006). The Sedom Fm. salts were formed in the Ca-chloride brine of the Sedom Lagoon that intruded the Dead Sea Basin during the late Miocene (Starinsky, 1974; Stein, 2001; Gavrieli and Stein, 2006; Katz and Starinsky, 2009).

The evaporite units of the Sedom Fm. were mapped and described by Zak (1967). They comprise of slanted, overturned, and vertical orientated sequence of halite layers (77%), gypsum, anhydrite, and shale of marine origin (Fig. 1c). Topping the vertical evaporite layers is a mostly horizontal erosional unconformity capped by a ~40 m thick section of sedimentary residue abundant in anhydrite and gypsum, as well as marl, dolomite, and clastic material which was left in-situ, as insoluble residue, following the dissolution of halite (*caprock*; Fig. 1c).

The widespread dissolution of halite and formation of the caprock on Mount Sedom was suggested to have occurred in the subsurface (Vroman, 1950) at times when the lake transgressed over the western margins of the basin reaching the diapir (Zak, 1967). Zak (1967) suggested that the composition of the groundwater that dissolved the Sedom Fm. halite and formed the caprock was of Ca-Chloride type, saturated with respect to gypsum, as the caprock contains abundant sulfate evaporite minerals, which would have been dissolved completely by freshwater.

3. Methods

3.1. Sampling

A general description of the DSDDP core at 5017-1-A is given by Neugebauer et al. (2014) and the chronology of the core is given by Torfstein et al. (2015) and Kitagawa et al. (2017). Detrital sediment samples, 15–30 ml in volume, and numbering 126 in total, were collected during the drilling campaign of 2010/11 at intervals of several centimeters to 14.5 m from core catcher sections, and during 2013 at similar intervals but from accompanying core sections. The samples were kept airtight to prevent evaporation and indeed no significant variability was observed between chemical concentrations of core catcher and core section samples (Levy et al., 2017). Pore fluid was obtained from core catcher samples by centrifuge extraction, and from core section samples by hydraulic press fluid extraction.

Table 1
δ^{37}Cl results from core 1A pore fluids (Cl^-) and halites, Dead Sea brine and halite, and halites from Mount Sedom.

Sample type	Location:	ID#	Core depth (m blf)	Age (ka)	±	δ^{37}Cl (‰)	±	Notes
Pore fluid	Core 5017_1A	1-A-12_1	21.6	2.8	0.1	−0.15	0.1	
Pore fluid	Core 5017_1A	1-A-46_3	99.8	16.8	0.6	−0.12	0.1	
Pore fluid	Core 5017_1A	1-A-49_4	108.9	22.4	0.6	−0.21	0.06	
Pore fluid	Core 5017_1A	1-A-56_4	130.3	36.6	1.3	−0.2	0.06	
Pore fluid	Core 5017_1A	1-A-61_4	145.5	46.7	1.7	0.06	0.09	
Pore fluid	Core 5017_1A	1-A-69_4	166.9	61.9	2.4	−0.51	0.11	
Pore fluid	Core 5017_1A	1-A-69_4	166.9	61.9	2.4	−0.39	0.06	
Pore fluid	Core 5017_1A	1-A-77_1	190.2	74.9	3.4	−0.37	0.11	
Pore fluid	Core 5017_1A	1-A-80_4	200.4	85.7	3.7	−0.31	0.1	
Halite	Core 5017_1A	1-A-81_2	202.9			−0.18	0.07	Small cumulate crystals (SC)
Halite	Core 5017_1A	1-A-81_2	202.9			−0.05	0.07	Duplicate sample
Halite	Core 5017_1A	1-A-91_2	234.1			0.03	0.08	Small cumulate crystals (SC)
Pore fluid	Core 5017_1A	1-A-92_2	235.3	116.7	5.2	−0.46	0.1	
Halite	Core 5017_1A	1-A-100_3	256.1			0.06	0.1	Small cumulate crystals (SC)
Halite	Core 5017_1A	1-A-100_3	256.1			0.06	0.1	Large bottom growth crystals (LC)
Pore fluid	Core 5017_1A	1-A-100_5	256.2	119.3	2.8	−0.28	0.06	
Pore fluid	Core 5017_1A	1-A-100_5	256.2	119.3	2.8	−0.37	0.07	Duplicate sample
Pore fluid	Core 5017_1A	1-A-109_3	282.8	122.6	1.4	−0.17	0.1	
Pore fluid	Core 5017_1A	1-A-122_4	316.2	131.6	1.1	−0.17	0.1	
Brine	Dead Sea					−0.30	0.09	Taken in 2013 at 100 m depth.
Brine	Dead Sea					−0.32	0.03	Taken in 2013 at 100 m depth (Duplicate)
Halite	Dead Sea					0.02	0.10	Precipitated from 2013 Dead Sea brine
Halite	Mount Sedom	Mearat Sedom 1				0.29	0.09	From Mearat Sedom Mbr.
Halite	Mount Sedom	Mearat Sedom 2				0.00	0.11	From Mearat Sedom Mbr.
Halite	Mount Sedom	Lot 1				0.34	0.08	From Lot Mbr.
Halite	Mount Sedom	Lot 2				−0.10	0.04	From Lot Mbr.
Halite	Mount Sedom	Lot 3				0.10	0.06	From Lot Mbr.
Halite	Mount Sedom	Lot 4				0.12	0.06	From Lot Mbr.

Four halite samples from the core were collected and analyzed for δ^{37}Cl (see Table 1). Additionally, four halite samples (0.5–1 kg in weight) were collected from the Lot Member (Mbr.) and two from the Me'arat Sedom Mbr. of the Mount Sedom diapir (see Table 1). Modern Dead Sea brine was collected using a Niskin bottle from the center of the lake at 100 m depth in February 2013 (Golan et al., 2016), and was subsequently used in this study for determining the δ^{37}Cl fractionation during halite precipitation (see Table 1). The modern Dead Sea brine was transferred into an air-tight 1.5 liter (L) bottle and kept at room temperature. Due to super-saturation at the time of sampling subsequently halite crystals precipitated within the bottle (see supplementary Fig. 1). Both the brine and crystals were extracted from the bottle in February 2016 and analyzed for δ^{37}Cl.

3.2. Chemical and isotope analyses

Major cation (Na^+ and Mg^{2+}) concentrations were analyzed using ICP–AES. Br^- and Cl^- concentrations were analyzed by ICP–MS, and titration, respectively (C.B.E. ± <5%) (see supplementary Table 1). δ^{37}Cl isotope analyses were carried out at the University of Waterloo, Canada following the procedure described in Shouakar-Stash et al. (2005). Inorganic Cl^- was precipitated from solutions as silver chloride (AgCl) by adding silver nitrate to the solution. The precipitate was then reacted with methyl iodide (CH_3I) to form CH_3Cl. Following separation of CH_3I from CH_3Cl, duplicate samples of CH_3Cl were analyzed on CF-IRMS (Micromass IsoPrime). The results are presented in the permil notation (Eq. (1); see Table 1):

$$\delta^{37}\mathrm{Cl} = \left[\left({}^{37}\mathrm{Cl}/{}^{35}\mathrm{Cl}_{\mathrm{sample}}\right)/\left({}^{37}\mathrm{Cl}/{}^{35}\mathrm{Cl}_{\mathrm{SMOC}}\right) - 1\right] \times 1000(‰) \quad (1)$$

The standard being Standard Mean Oceanic Chloride (SMOC; i.e. $\delta^{37}\mathrm{Cl}_{\mathrm{SMOC}} = 0‰$), and the precision of the duplicate measurements is better than ±0.10‰.

^{37}Cl isotope fractionation during halite precipitation from Dead Sea brine was derived from the difference between the δ^{37}Cl of all measurements of halite and the Cl^- in the brine (i.e. $\Delta = \delta^{37}\mathrm{Cl}_{\mathrm{NaCl}} - \delta^{37}\mathrm{Cl}_{\mathrm{Cl^-}}$) and averaged (see supplementary Table 2), following the procedure in Eggenkamp et al. (2016).

3.3. Calculations of the degree of saturation for halite

The degree of saturation with respect to halite of the pore fluid samples ($\Omega_{\mathrm{NaCl}} = \mathrm{IAP}/\mathrm{K}_{\mathrm{NaCl}}$) was determined using the Pitzer approach and database for high salinity solutions integrated within PHREEQC© software (Pitzer, 1973; Parkhurst and Appelo, 1999). Brine density for pore fluid samples was estimated using the empirically determined equation calculated for natural brines in and around the Dead Sea at similar temperature and salinity ranges of the pore fluids (Zilberman-Kron et al., 2017; see supplementary Fig. 2). A halite saturation curve ($\Omega_{\mathrm{NaCl}} = 1$; Fig. 4) was created in PHREEQC© following the procedure detailed in Kiro et al. (2017).

3.4. Age estimation of core sediments

The published anchor age model for ICDP core 1A which is based on the integration of radiocarbon ages (on organic debris, Kitagawa et al., 2017), U–Th ages (measured on aragonites) and δ^{18}O (aragonite) stratigraphy tied to the $\delta^{18}\mathrm{O}_{\mathrm{Benthic}}$ LR04 and Soreq Cave δ^{18}O speleothem curves (see supplementary material in Torfstein et al., 2015 for full details), was used to convert depth (m blf) to age (ka) for sediments below >91 mblf (older than 14.5 ka). See data repository material in Levy et al. (2017) for more information.

4. Results

The abundant impermeable halite layers found in the core sedimentary record along with the high viscosity of the accompanying pore fluids significantly hampered subsurface chemical diffusion in

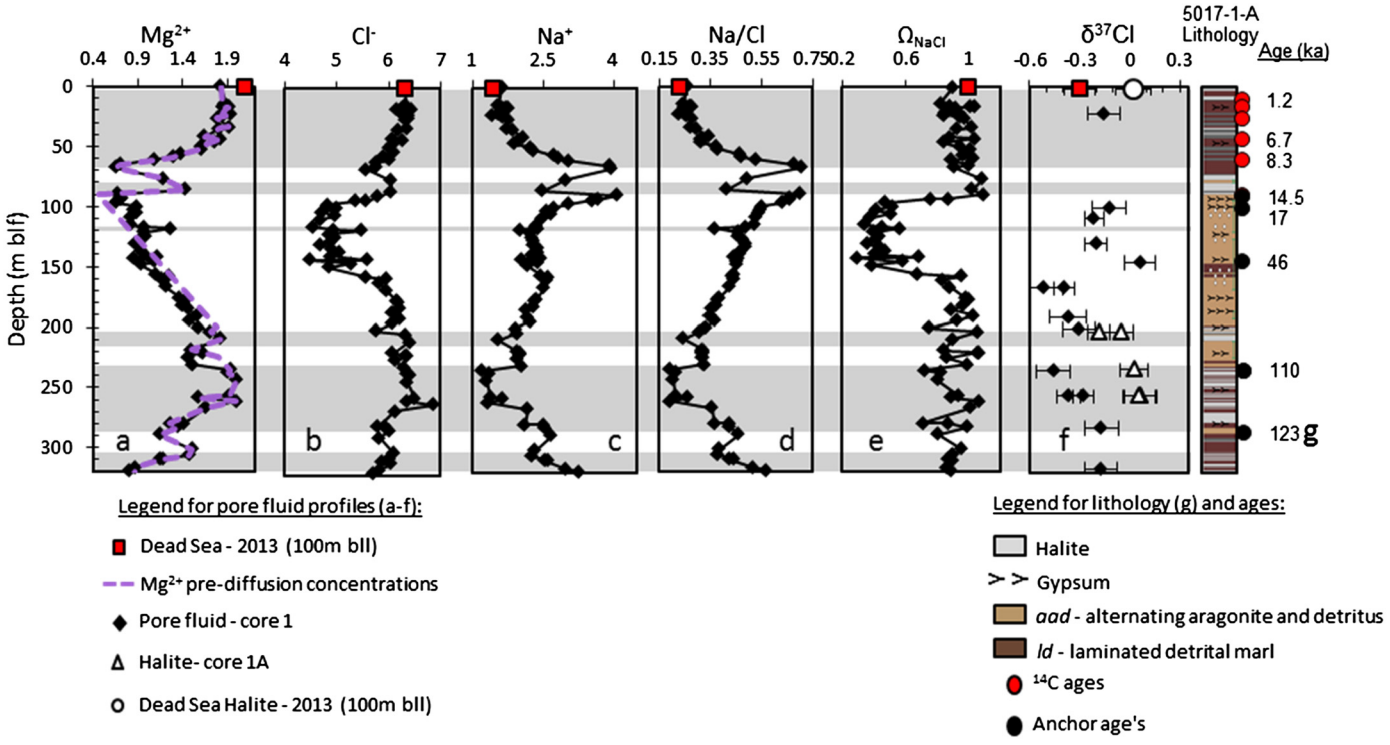

Fig. 3. ICDP core 5017-1-A pore fluids depth profiles and sediments (upper 320 m blf). From left to right (a–d after Levy et al., 2017): (a) Mg^{2+} (mol/L), where purple dotted line represents the pre-diffusion concentration values from diffusion model estimation; (b) Na^{+} (mol/L); (c) Cl^{-} (mol/L); (d) Na/Cl; (e) Ω_{NaCl}; (f) $\delta^{37}Cl$ of pore fluid Cl^{-} (black diamonds), halite (white triangles), and halite precipitated from Dead Sea brine (white circle). Red square – Dead Sea brine from 2013 at 100 m depth. Depth intervals showing a general decrease in Na/Cl are highlighted in grey, while intervals with Na/Cl increase are white; (g) Lithology of the core by Neugebauer et al. (2014), ^{14}C ages, and anchor ages (after Torfstein et al., 2015). (For interpretation of the references to color in this figure legend, the reader is referred to the web version of this article.)

the upper 320 m blf interval of the core (ca. 132 ka). This is evident by the retention of the long-term concentration trends of Mg^{2+} (Fig. 3a – black) in comparison to pre-diffusion modeling concentration estimates in Levy et al. (2017) (Fig. 3a – purple). Given the retention of the Mg^{2+} profile, the long term trends of non-conservative Na^{+} and Cl^{-} concentrations (Fig. 3b and 3c) and the Na/Cl ratio (Fig. 3d) call for a detailed study.

The degree of saturation with respect to halite within the intervals of 320–156 m blf (ca. 132 ka–54 ka) and 94–0 m blf (ca. 15–0 ka) were found to be slightly undersaturated to supersaturated with respect to halite ($\Omega_{NaCl} = 0.80 - 1.09$) for >90% of pore fluid samples (Fig. 3e). In comparison, within the interval of ~149–100 m blf (ca. 49 ka–17 ka) pore fluids were calculated to be much more undersaturated with respect to halite ($\Omega_{NaCl} = 0.29–0.56$; Fig. 3e).

The $\delta^{37}Cl$ of pore fluid Cl^{-} (black diamonds in Fig. 3f; see Table 1) range between −0.55‰ to +0.06‰, with the vast majority depleted relative to SMOC. Between 316 and 235 m blf (ca. 132–117 ka), at an interval with layered halite in the core, there is an upward increase in Mg^{2+} concentrations, a drop in Na/Cl, and a gradual decrease in $\delta^{37}Cl$ from −0.17‰ (±0.10) to −0.46‰ (±0.10). $\delta^{37}Cl$ values from halite layers (white triangles in Fig. 3f) at 235 m blf and 256 m blf are relatively enriched with respect to ^{37}Cl in the pore fluids at similar depths. Halite crystals with different morphologies (i.e. *small cumulate* type and *large crystal* type; Kiro et al., 2016) at 256 m blf depth provide a similar value of $\delta^{37}Cl = +0.06‰$ (±0.10). Between 200–90 m blf, an interval free of halite, there is a general enrichment of pore fluid $\delta^{37}Cl$.

$\delta^{37}Cl$ in the modern Dead Sea brine (2013) is −0.30‰ (±0.09) (red square in Fig. 3f at 0 m; and Table 1). Halite crystals precipitated at room temperature from this brine gave values of $\delta^{37}Cl = +0.02‰$ (±0.10), noticeably enriched in $\delta^{37}Cl$ compared to the precipitating solution. The $\delta^{37}Cl$ values of two samples from the Me'arat Sedom Mbr. at Mount Sedom and the four samples from the Lot Mbr. at Mount Sedom can be found in Table 1.

5. Discussion

5.1. Chemical and $\delta^{37}Cl$ isotope variations during halite precipitation and dissolution: 'rules of the game'

Mg^{2+} and Br^{-} are conservative in the Dead Sea pore fluids (Levy et al., 2017; see supplementary Fig. 3) and the trends of Mg^{2+} concentrations observed in the pore fluid profile is a manifestation of water balance changes, or the net addition/removal of H_2O (Levy et al., 2017; Fig. 3a). The long-term net water balance changes in the Dead Sea are inherently the result of precipitation and evaporation changes in the Dead Sea watershed and follow a glacial–interglacial pattern. Thus, the conservative Mg^{2+} and Br^{-} concentration records show a cyclic glacial–interglacial pattern as also observed, for example, in the atmospheric CO_2 record from ice cores (Fig. 2).

Mg^{2+} concentrations (mol/Kg_{H2O}) in the pore fluid samples that are inversely normalized to the sample found at 235.3 m blf/ca. 117 ka (i.e. $[Mg^{2+}_{t=117\,ka}]/[Mg^{2+}_{t}]$), can be used to gauge the relative degree of dilution, or the inverse of the degree of evaporation, to that sample which is at peak concentration (Levy et al., 2017). Na^{+} and Cl^{-} however are non-conservative, and relative change in concentrations have been influenced by both net water balance changes and other processes, such as dissolution and precipitation of halite over time. Plotting the $[Mg^{2+}_{t=117\,ka}]/[Mg^{2+}_{t}]$ ratio against Na/Cl of pore fluid samples provides a robust assessment of the halite precipitation and dissolution mechanism in response to net water balance changes and lake level changes (Fig. 4a – inset).

During lake level drop and brine concentration the $[Mg^{2+}_{t=117\,ka}]/[Mg^{2+}_{t}]$ ratio would decrease (purple arrow's in Fig. 4a – inset)

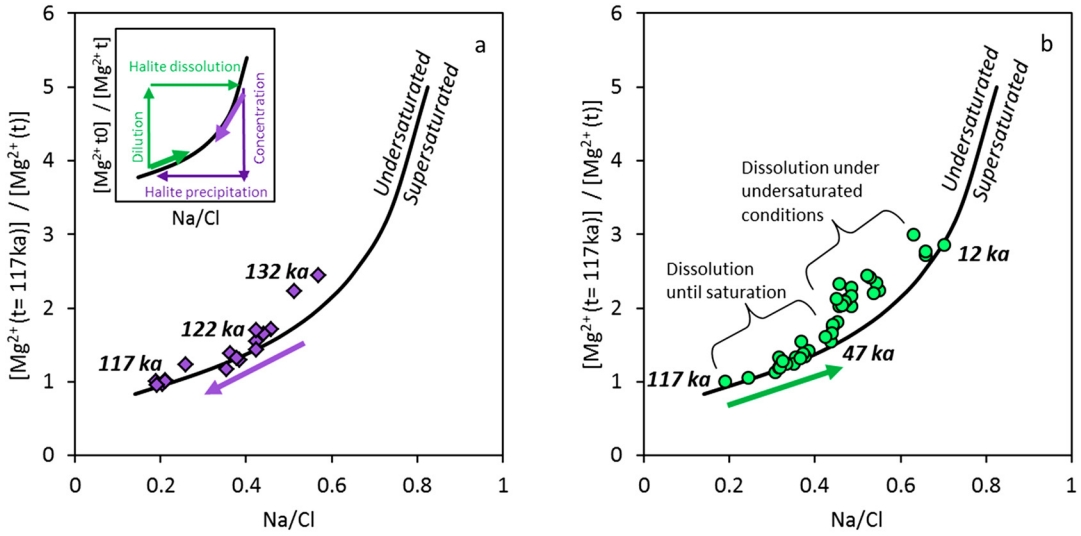

Fig. 4. Brine dilution/concentration and halite dissolution/precipitation ($[Mg^{2+}_{t=117\,ka}]/[Mg^{2+}_{t}]$ vs. Na/Cl) for pore fluids from: (a) last interglacial period during which concentration and halite precipitation took place (purple diamonds). (b) last glacial period with dilution and halite dissolution (green circles). The halite saturation curve ($\Omega_{NaCl} = 1$; black line) was calculated for the dilution of the pore fluid sample at ~117 ka (235 mblf). The key inset at the top left of (a) is a schematic representation of the impact of dilution followed by halite dissolution (green arrows), and concentration followed by halite precipitation (purple arrows). (For interpretation of the references to color in this figure legend, the reader is referred to the web version of this article.)

until the brine reaches saturation with respect to halite (black curve) and halite precipitation would then commence. From here a continued lake level drop, or negative water balance, would result in halite precipitation and in the decrease of both the $[Mg^{2+}_{t=117\,ka}]/[Mg^{2+}_{t}]$ ratio and the Na/Cl ratio, moving downwards along the saturation curve. In contrast, during lake level rise and brine dilution the $[Mg^{2+}_{t=117\,ka}]/[Mg^{2+}_{t}]$ ratio would increase and the Na/Cl ratio would also increase given halite dissolution (green arrows in inset). If an excess supply of halite is available for dissolution, and there is no dissolution kinetic barrier, the brine should remain saturated with respect to halite during dilution, and graphically the brine would evolve upwards along the saturation curve. However, given a shortage of halite for dissolution during dilution the brine would be pushed into the undersaturated region and away from the saturation curve.

Pore fluid samples pertaining to the last interglacial (ca. 132–117 ka) predominantly record brine concentration and halite precipitation as evident by the decrease in the $[Mg^{2+}_{t=117\,ka}]/[Mg^{2+}_{t}]$ and Na/Cl ratios, respectively, with samples close to the calculated saturation curve (Fig. 4a). In contrast samples from the last glacial period record brine dilution and halite dissolution, as evident by increases in the $[Mg^{2+}_{t=117\,ka}]/[Mg^{2+}_{t}]$ and Na/Cl ratios, respectively. Samples from the early glacial are close to the saturation curve, inferring a process of dissolution of halite until saturation, while samples from the late glacial are undersaturated with respect to halite, suggesting deficiency of halite for dissolution to reach and maintain saturation.

In addition to the chemical compositions, the $\delta^{37}Cl$ isotope composition in the residual brine is expected to change as a result of halite precipitation and dissolution. Numerous experimental studies were conducted in which both natural and synthetic NaCl saturated solutions were evaporated to determine the ^{37}Cl fractionation in the precipitating halite crystals (i.e. Eggenkamp et al., 1995, 2016; Luo et al., 2012, 2014). In the study by Eggenkamp et al. (1995) NaCl saturated solutions were placed in a fumehood at 22 °C and allowed to precipitate halite crystals. This study found ^{37}Cl isotope fractionation of $\alpha_{(NaCl\text{-}solution)} = 1.00026 \pm 0.00007$ (1σ), and confirmed the preferential incorporation of ^{37}Cl isotope in the halite crystals. Eggenkamp et al. (2016) re-confirmed this value with a fractionation factor of $\alpha_{(NaCl\text{-}solution)} = 1.00035 \pm 0.00008$ (1σ). Luo et al. (2012) calculated individual fractionation factors for salt and brine samples collected during the entire evaporation process for brine of the saline Qarhan Lake (China) and, averaged over the course of evaporation, found $\alpha_{(NaCl\text{-}solution)} = 1.00045 \pm 0.00024$ (2σ) and 1.00048 ± 0.00018 (2σ) (Luo et al., 2012). A later study by Luo et al. (2014) using similar methods but synthetic NaCl saturated solution found slightly larger fractionation with $\alpha_{(NaCl\text{-}solution)} = 1.00055 \pm 0.00046$ (1σ) but with a larger standard deviation (Luo et al., 2015; Eggenkamp, 2015).

The above range of fractionation factors infer that given significant halite precipitation the $\delta^{37}Cl$ of the residual Cl^- in the brine and in the precipitating halite would decrease with ongoing precipitation as a result of isotope fractionation, along a Rayleigh distillation curve (i.e. Eggenkamp et al., 1995). Unlike halite precipitation, halite dissolution involves no isotope fractionation and the $\delta^{37}Cl$ in the solution will carry an increasing fraction of the isotope signature of the halite being dissolved. Due to the unique composition and environmental conditions of the Dead Sea the ^{37}Cl fractionation during halite precipitation was determined again but for the Dead Sea. This was done by calculating the difference between the $\delta^{37}Cl$ of the Dead Sea brine sample taken during 2013 and the halite crystals that precipitated in the brine following sampling at room temperature (i.e. $\Delta = \delta^{37}Cl_{NaCl} - \delta^{37}Cl_{Cl^-}$ (‰)) providing a result of $\Delta = +0.32$ (± 0.12) (i.e. $\alpha_{(NaCl\text{-}solution)} = 1.00032 \pm 0.00012$ (1σ)) (see supplementary Table 2). This value fits closely with the fractionation factors in the aforementioned studies (Eggenkamp et al., 1995, 2016; Luo et al., 2012, 2014).

Based on the determined fractionation value, the evolution of $\delta^{37}Cl$ composition of the brine and precipitating halite can be calculated using Rayleigh distillation equations. These equations estimate the $\delta^{37}Cl$ of the residual Cl^- in the lake ($\delta^{37}Cl_{Cl\text{-}DIST}$) and the contemporaneous precipitating halite ($\delta^{37}Cl_{NaCl\text{-}DIST}$) as a function of f_{Cl^-}, i.e. the mol fraction of the original dissolved Cl^- reservoir still remaining in the brine (eq. (2) and eq. (3), respectively):

$$\delta^{37}Cl_{Cl\text{-}DIST} = \delta^{37}Cl_{Cl(0)} + \Delta \cdot \ln(f_{Cl^-}) \quad (2)$$

$$\delta^{37}Cl_{NaCl\text{-}DIST} = \delta^{37}Cl_{Cl\text{-}DIST} + \Delta \quad (3)$$

where $\delta^{37}Cl_{Cl(0)}$ is the initial isotope composition of the brine prior to the onset of halite precipitation (i.e. at $f_{Cl^-} = 1$). It should

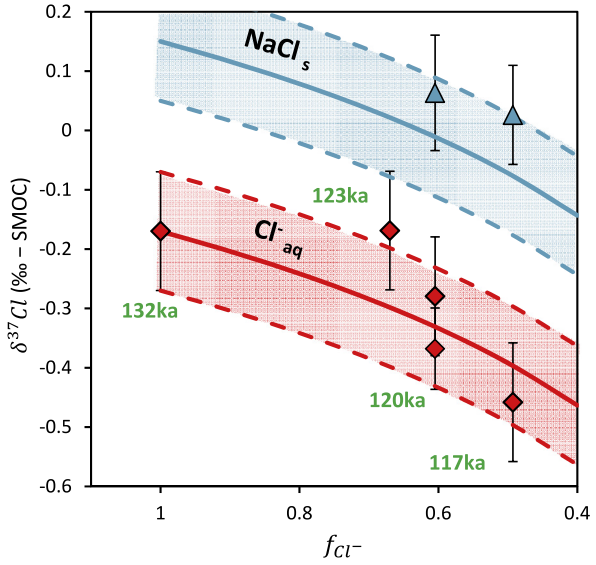

Fig. 5. Evolution of δ^{37}Cl isotope composition of brines in the Last Interglacial Dead Sea (bottom curve in red) and halite (upper curve in blue) as a result of halite precipitation, following the Rayleigh distillation equations (eqs. (2) and (3); $\delta^{37}Cl_{Cl(0)} = -0.17$, $\Delta = 0.32‰$). Red diamonds: δ^{37}Cl values of pore fluid Cl^-, blue triangles: δ^{37}Cl values of halites. Dotted curves represent the standard deviation of initial brine composition of ± 0.10‰. (For interpretation of the references to color in this figure legend, the reader is referred to the web version of this article.)

be noted that with increasing evaporation and change in composition, additional Cl^- minerals may begin to precipitate. For eqs. (2) and (3) to be valid the lower limit of f_{Cl^-} should be determined such that it allows the brine to evolve until the first non-halite Cl^- bearing mineral starts precipitating. In the case of the Dead Sea brine this mineral is carnallite ($MgKCl_6 \cdot H_20$). The calculated Rayleigh distillation curves of eqs. (2) and (3) for brines precipitating halite in a closed system with $\delta^{37}Cl_{Cl(0)} = -0.17‰$ and $\Delta = 0.32‰$ can be seen in Fig. 5.

Based on the above defined 'rules of the game' and observations for changes in chemical and δ^{37}Cl isotope compositions, the evolution of the Cl^- reservoir in the lake is investigated for the time interval of the last interglacial (ca. 132–117 ka) and the last glacial periods (ca. 117–17 ka).

5.2. The last interglacial period (132–117 ka)

Layered halite that precipitated during the lake level drops of the last interglacial period (MIS5e) form over ~30 m of recovered halite over ~85 m of drilling in the DSDDP deep core (~330–235 m depth). Detrital layers of varying thickness fill most of the non-halite intervals, and indicate changes in the lake hydrology forced by increased regional hydrological-climate activity (Kiro et al., 2016; Palchan et al., 2017). One prominent example of ~23 m thick halite-free detrital layer found at ~303–280 m depth in the core (ca. 128–122 ka) was inferred to have been formed by a bout of humid regional climate conditions which prevented evaporite layer precipitation (Torfstein et al., 2015).

Based on modern observations of the Dead Sea hydrology, Kiro et al. (2017) estimated that spanning the last interglacial period there was a relatively negligible flux of *external* Cl^- and Mg^{2+} ions into the lake with relation to the thickness of halite in the core (i.e. contributions from the Jordan river, brine springs, and dissolution of halite on Mount Sedom). In their paper during lake level drops in the last interglacial newly exposed halite deposits at the lake's beaches were believed to have been shifted to the deep lake from as part of the salt 'focusing' process, which remobilized Cl^- ('internal' source). One way to address the whether external source of Cl^- to the lake was negligible during that time is to assess whether there was Rayleigh distillation of δ^{37}Cl during halite precipitation. Rayleigh distillation assumes *closed* limnological conditions with respect to addition of external Cl^- into the lake but *open* conditions that allow for the removal of Cl^- from the brine as halite.

The possibility of Rayleigh distillation of δ^{37}Cl in the residual brine over this period was assessed by comparing δ^{37}Cl of Cl^- in pore fluids and of the halite in the core. For the Rayleigh distillation equations (eqs. (2) and (3)), $\delta^{37}Cl_{Cl(0)}$ was set as −0.17‰ (±0.10) or the pore fluid sample found at the start of the last interglacial at $t_0 = 132$ ka (316 m blf in core). f_{Cl^-} was calculated assuming the change in lake volume is relative to change in the concentration of conservative Mg^{2+} (following Kiro et al., 2017):

$$V_t = \frac{[Mg_0^{2+}]}{[Mg_t^{2+}]} \cdot V_0 \tag{4}$$

where V_0 and Mg_0^{2+} are the respective volume and Mg^{2+} concentrations at time t_0, or the start of the last interglacial at ca. 132 ka, and V_t and Mg_t^{2+} respectively for time t during the last interglacial. Multiplying V_t (eq. (4)) with pore fluid Cl^- concentration at similar time interval (Cl_t^-) provides estimations for the bulk inventory (mol) of Cl^-. Thus, $f_{Cl^1,t}$ (mol Cl_t^-/mol Cl_0^-) can be estimated for any sample in the pore fluids:

$$f_{Cl^-,t} = \frac{[Cl_t^-]}{[Cl_0^-]} \cdot \frac{[Mg_0^{2+}]}{[Mg_t^{2+}]} \tag{5}$$

While f_{Cl^-} (eq. (5)) decreases during halite precipitation it may also yield $f_{Cl^-} > 1$ or an evident increase in total dissolved Cl^- in the brine above the reference Cl^- value (Cl_0^-) as an indication of halite dissolution.

Using Eq. (5) pore fluid samples in the studied interval were plotted on the Rayleigh distillation curve in Fig. 5. The results show that between ca. 132 and 117 ka the δ^{37}Cl of pore fluids decreased with decreasing f_{Cl^-} and time, and mostly lie within the calculated Rayleigh distillation curve area (red area in Fig. 5; Eq. (2)). Halite samples that are relatively enriched in δ^{37}Cl in comparison to corresponding pore fluids at similar depths are also situated in the upper Rayleigh distillation curve area for halite (blue area in Fig. 5; Eq. (4)). Note that f_{Cl^-} for these two halite samples were assumed to be those of the pore fluids at similar depths (see Table 1).

The δ^{37}Cl variability of samples in comparison to the Rayleigh model can be attributed to analytical limitations, but also to natural processes, such as halite dissolution. For example, in Fig. 5 the pore fluid sample corresponding to ca. 123 ka has the same δ^{37}Cl as the previous value at ca. 132 ka ($\delta^{37}Cl = -0.17‰ \pm 0.1$), albeit the decrease in f_{Cl^-}, and as such could be an indication of localized dissolution of halite in addition to halite precipitation. Nevertheless, altogether the data fits a Rayleigh distillation model given the relatively large standard deviation of analysis ($1\sigma = \sim 0.1‰$), and for this reason the effects of halite dissolution appear to be negligible over the entire time interval. Thus in addition to Mg^{2+}, there was relatively negligible influx of external Cl^- into the lake inventory during the last interglacial (MIS5e) period.

5.3. The end of the last interglacial and last glacial periods (ca. 117–17 ka)

During the final stages of the last interglacial period and throughout the last glacial period the conservative Mg^{2+} ion shows a continuous decrease along with simultaneous enrichment of Cl^- and Na^+, as represented by the Na/Cl ratio (Fig. 6a). From the end

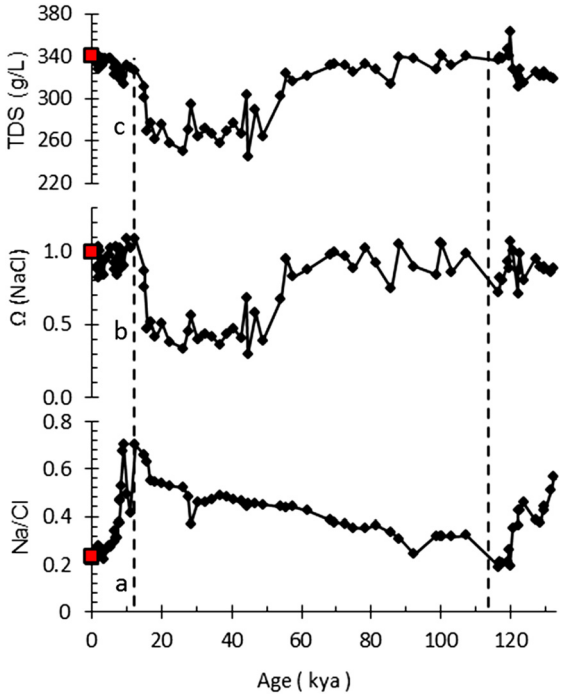

Fig. 6. Pore fluid chemistry (black dots) since 133 ka: (a) Na/Cl; (b) Ω_{NaCl}; (c) TDS (g/L; supplementary Table 1). The last glacial interval is shown between the dotted lines. The Dead Sea chemical composition of 2013 is shown as a red square for reference. (For interpretation of the references to color in this figure legend, the reader is referred to the web version of this article.)

of MIS5e at ca. 117 ka until 54 ka pore fluids are close to saturation with respect to halite (Fig. 6b). Apart from a brief interval at ca. 92 to 85 ka (210–200 m blf) where Mg^{2+} concentrations increases, Na/Cl ratio decreases and halite had precipitated, the general trend shows dilution and increasing Na/Cl ratio. The pore fluids from the last glacial Lake Lisan (ca. 49 ka–17 ka) also show evidence of continued dissolution but are undersaturated with respect to halite ($\Omega_{NaCl} = 0.29–0.56$). At that unique time interval, where there is a decrease in salinity (Lazar et al., 2014) but continuous dissolution of halite, the rate of lake dilution must have exceeded the rate of halite dissolution.

Clearly halite dissolution had significant influence on the salinity of the last glacial lake (Fig. 6c). The observations in the pore fluids corroborate previous results from the aragonite laminae sequences of the exposed terraces of the last glacial Lisan Fm., showing an increase in Na/Ca ratio over time, and suggested to be the result of increasing salinity in the upper epilimnic layer of Lake Lisan (Katz et al., 1977; Begin et al., 2004).

During the time-interval of ca. 49 ka–17 ka the lake reached its highest stand (Bartov et al., 2003) and the pore fluids were undersaturated with respect to halite, and at this interval a first order approximation for the rate of Cl^- enrichment in the lake brine can be calculated. Limnological constraints (lake stratification) are ignored as there is evidence of salinity enrichment in both the upper and lower lake. The lake volume V_t for each respective pore fluid sample over that period was calculated using eq. (4) where initial conditions for Mg_0^{2+} were assumed as modern 2013 Dead Sea concentration and V_0 as the modern Dead Sea volume estimated from the Dead Sea hypsometric curve provided in Hall (1996) for −428 m bmsl yielding 118 km^3 ($1.18 \cdot 10^{14}$ L). Multiplying the calculated volumes (V_t) by respective Cl^- concentrations in the pore fluids yields an average rate of Cl^- enrichment of $4 \cdot 10^{12}$ mol Cl^-/kyr (for ca. 49 ka–17 ka).

Two potentially significant sources of halite that could be dissolved upon the rise of Lake Lisan are: 1) halite deposits from the preceding last interglacial period along the lake's margins, and 2) the Mount Sedom salt diapir. Halite deposits from the preceding last interglacial period were shown to have been re-deposited in the center of the lake due to the salt 'focusing' process in the last interglacial (Kiro et al., 2017). Mount Sedom bears significant evidence of halite dissolution as shown by the caprock and indeed, the Na/Ca ratio from Lisan Fm. aragonite laminae, show systematic variations in the exposed terraces with higher values in southern exposures of the Lisan Formation, which suggest dissolution of the salt at Mount Sedom (Fig. 1c; Weinberger et al., 2007).

Table 2
Estimates for the rate of Cl^- enrichment in the lake from ca. 49–17 ka, the rate of halite exposure during uplift on the Mount Sedom diapir based on the 3 to 9 mm/yr range of uplift rates (Frumkin and Ford, 1995; Frumkin, 1996; Pe'eri et al., 2004; Weinberger et al., 2006, 2007), and the total halite dissolved on Mount Sedom based on 200 m 'dissolved' halite thickness (Zak, 1967).

		Unit
Rate of lake Cl^- enrichment (ca. 49–17 ka):	$4 \cdot 10^{12}$	mol/kyr
Rate of halite exposure during uplift of Mt. Sedom diapir:	$1.3 \cdot 10^{12}$–$4.0 \cdot 10^{12}$	mol/kyr
Total halite dissolved on Mt. Sedom diapir:	$1.2 \cdot 10^{14}$	mol

In order to assess whether Mt. Sedom halite could have been a significant source for the observed salinity enrichment of the last glacial Dead Sea, independent estimations for the exposure rate and quantity of the halite on Mt. Sedom were made and compared to our previous estimation for the rate and magnitude of Cl^- enrichment in the lake. For a first order approximation the specific location and mechanism of the halite dissolution occurred were ignored and it is assumed that the rate of halite dissolution on Mount Sedom was proportional to the diapir exposure rate and all halite dissolved on the diapir was transferred into the adjacent terminal lake.

Various uplift rates of the Sedom diapir have been measured or estimated. Interferometric synthetic aperture radar (InSAR) measurements of the diapir were used to determine the modern uplift rate of the diapir (Pe'eri et al., 2004; Weinberger et al., 2006) while morphological evidence found in salt caves and dating of cave levels using ^{14}C from twigs found in the alluvium within the caves determined the diapir's uplift during the Holocene (Frumkin and Ford, 1995; Frumkin, 1996). These methods yielded rates between 5 and 9 mm/yr. During the last glacial the overall uplift rate of Sedom diapir was estimated to be slightly lower at 3 mm/yr (Weinberger et al., 2006, 2007). Multiplying the range of uplift rates (3 to 9 mm/yr) by the surface area of the mountain (16 km^2) gives volumetric exposure rates from 0.048 to 0.144 km^3/kyr. As the Sedom Fm. comprises of 77% halite (Zak, 1967) this range was corrected from 0.037 to 0.111 km^3/kyr of halite. Multiplying by the density of Sedom salt (2115 kg/m^3; Zak, 1967) and dividing by the molecular weight of NaCl yields values of $1.3 \cdot 10^{12}$ to $4.0 \cdot 10^{12}$ mol/kyr, as first-order approximations for the exposure rates of the salt diapir. Additionally, the total halite dissolved on the diapir can be estimated according to amount of accumulation of caprock which was estimated to require dissolution of halite of 200 m thickness (Zak, 1967). The various estimates are provided in Table 2.

The independent calculations for the enrichment of Cl^- in the lake and exposure rate of halite on Mount Sedom yield values of similar magnitude ($\sim 10^{12}$ mol/kyr; Table 2). These first order approximations support the hypothesis that Mount Sedom was a major contributor of the Na^+, Cl^-, and salinity inventories in last glacial Lake Lisan. The larger value for the rate of enrichment in the pore fluids in comparison to halite exposure rate on Mount Sedom could be due to ICDP core proximity to the diapir and lo-

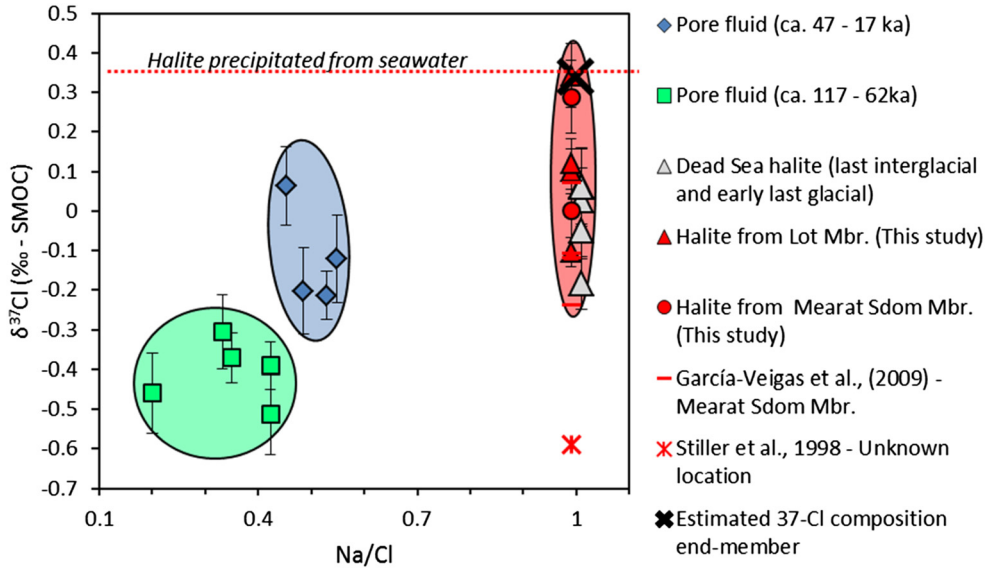

Fig. 7. δ^{37}Cl (‰) vs. Na/Cl. Data from pore fluids dating to ca. 117–62 ka (green) and ca. 47–17 ka (blue). Included are values for halite from Mt. Sedom (red) from both this study and literature (García-Veigas et al., 2009; Stiller et al., 1998). Also included is the estimated halite end member that was dissolved ($\delta^{37}Cl_{NaCl} = +0.34$‰; black cross) and estimated $\delta^{37}Cl_{NaCl}$ of halite precipitated in equilibrium from modern seawater ($\delta^{37}Cl_{NaCl} = +0.35$‰ – Eggenkamp et al., 2016; red dotted line). (For interpretation of the references to color in this figure legend, the reader is referred to the web version of this article.)

calized amplification. This is supported by the fact that the Na/Ca ratio in aragonite, an indicator of salinity in the last glacial lake, decreases with northward distance away from the Dead Sea and Mt. Sedom (Begin et al., 2004).

5.4. δ^{37}Cl as a tracer for halite dissolution

In the study by Stiller et al. (1998) the fluxes of freshwater and saline water into the modern (1982) Dead Sea were used to understand δ^{37}Cl changes. The freshwater and saline water end members showed relative variability of δ^{37}Cl values ranging from −0.37‰ (Ein Feshka spring) to +1.01‰ (Nahal Arugot). In comparison, the pore fluid compositions during last glacial period show clear evidence of Cl^- enrichment as a result of halite dissolution. It should be noted that halite dissolution is accompanied by no ^{37}Cl fractionation and thus the δ^{37}Cl in the dissolving solution will slowly inherit the isotope signature of the contributing halite being dissolved over time.

Fig. 7 presents δ^{37}Cl (‰) vs. Na/Cl of samples from this and other studies of the Dead Sea and Mount Sedom. With halite dissolution (increasing Na/Cl) and time, pore fluids generally became enriched in δ^{37}Cl. Added to the graph are the possible solutions which had dissolved halite (Na/Cl = 1) with values from Mount Sedom and halite from the last interglacial which would have been available at the marginal terraces. Bulk halite samples from the Lot and Me'arat Sedom Mbr. of the Sedom diapir measured in this study provide a range of −0.10‰ to +0.34‰ (Fig. 7; see Table 1). However, a study by García-Veigas et al. (2009) found a range of δ^{37}Cl from halite of the Me'arat Sedom Mbr. of −0.24‰ to +0.07‰ and Stiller et al. (1998) measured a δ^{37}Cl sample from an unknown location at the Mount Sedom salt diapir at −0.59‰. Thus, while the Mount Sedom salt diapir is of marine origin and precipitated in a lagoon environment, its δ^{37}Cl composition shows significant heterogeneity inferring changing evaporation stages of seawater in its Miocene paleo-environment where it had formed. The δ^{37}Cl variability observed in the evolving pore fluids over the last glacial could therefore be due to changing δ^{37}Cl composition of halite being dissolved. Nevertheless over the last glacial there is clearly a δ^{37}Cl enrichment in the pore fluids and an approximation for the average δ^{37}Cl composition of the dissolved halite ($\delta^{37}Cl_{NaCl}$) was made by a simple mass balance calculation (eq. (6)):

$$\delta^{37}Cl_{Cl^-,17\,ka} \times f_{Cl^-,17\,ka} = \delta^{37}Cl_{Cl^-,117\,ka} + \left(\delta^{37}Cl_{NaCl} \times (f_{Cl^-,17\,ka} - 1)\right) \quad (6)$$

Based on eq. (5) the relative enrichment of the Cl^- reservoir between ca. 117 to 17 ka was calculated to be ~73% ($f_{Cl^-,17\,ka} = 1.73$) and eq. (6) yields $\delta^{37}Cl_{NaCl} = +0.34$‰. This estimation is enriched in δ^{37}Cl in comparison to the range of halite precipitated in the Dead Sea during the preceding last interglacial and early last glacial (δ^{37}Cl = −0.18‰ to +0.06‰) and very close to the theoretical δ^{37}Cl of halite which would have precipitated in equilibrium from evaporated seawater of δ^{37}Cl = +0.35‰ (based on the fractionation factor determined by Eggenkamp et al., 2016). The estimation provides an additional support for Mount Sedom as the source halite that dissolved into the late Pleistocene Dead Sea and replenished its Na^+ and Cl^- inventories.

6. Summary and conclusions

Halite precipitation and dissolution in the Late Pleistocene Dead Sea had occurred as a response to water balance changes which were inherently related to regional climate changes. During periods of lake level drops and brine concentration, characteristic of the last interglacial (ca. 132–117 ka) concentrations (e.g. Mg^{2+}) increased until the brine reached saturation with respect to halite, and halite precipitation commenced leading to a decrease in the Na/Cl ratio. The δ^{37}Cl of Cl^- in the residual brine and in the halite decreased with ongoing time and followed a Rayleigh distillation curve as a result of isotope fractionation, with >50% of Cl^- removed during this process. Thus the lake behaved as a *closed* limnological system with negligible external sources of Cl^-. In contrast, during the lake level rise of the last glacial, the salinity was controlled by the rate of lake dilution and dissolution of accessible halite, mostly from the rising Mount Sedom salt diapir. For the early part of the last glacial (ca. 117 ka–54 ka) the brine was close to halite saturation, indicating that halite was present to maximize the potential of dissolution. Later on (ca. 49–17 ka) the deep lake became undersaturated with respect to halite albeit continued dissolution as lake dilution exceeded the rate of halite dissolution.

First order estimations for the rate of Cl^- enrichment in the lake and halite exposure on the Mt. Sedom salt diapir yield values of similar magnitude ($\sim 10^{12}$ mol/kyr) and support the hypothesis that halite on Mt. Sedom was the major contributor of Cl^-.

Similar processes can occur in other environments where salt-bodies are dissolved leading to significant salinity changes in the adjacent water-bodies. By assessing the chemical and $\delta^{37}Cl$ compositions of pore fluids and halite, it is possible to reconstruct the composition of the residual halite precipitating brine over time, as well as determine and quantify sources of halite dissolution.

Acknowledgements

We wish to thank Chongguang Luo, Hans Eggenkamp, an anonymous reviewer, and the editor for their reviews that considerably improved the paper. We wish to sincerely thank I. Swaed from the Geological Survey of Israel (GSI), E. Eliani-Russak, M. Adler, I. Bar-Or, N. Avrahamov, and A. Russak from Ben-Gurion University of the Negev, and G. Antler from Aarhus University for help in core catcher sampling and analysis. D. Stiber, G. Sharabi, O. Berlin and other members of the GSI geochemical division carried out major ion analysis. The Environmental Isotope Laboratory at the University of Waterloo (ON, Canada) for carrying out $\delta^{37}Cl$ isotope analyses. M. Stiller for helpful discussion on the $\delta^{37}Cl$ system in the lake. R. Weinberger (GSI) and I. Haviv (BGU) for ample advice and discussion of Mount Sedom and S. Stein and N. Amiel for help in sampling Mount Sedom. The study is supported by an Excellence Center of the Israel Science Foundation grant 1736/11 to Lazar.

Appendix A. Supplementary material

Supplementary material related to this article can be found online at https://doi.org/10.1016/j.epsl.2018.02.003.

References

Agnon, A., Weinberger, R., Zak, I., Sneh, A., 2006. Geological Map of Israel 1:50,000: Sedom Sheet 20-1, 2. Geological Survey, Ministry of National Infrastructures. www.gsi.gov.il. (Accessed 15May2017).

Bartov, Y., Goldstein, S., Stein, M., Enzel, Y., 2003. Catastrophic arid episodes in the Eastern Mediterranean linked with the North Atlantic Heinrich events. Geology 31, 439–442. https://doi.org/10.1130/0091-7613(2003)031<0439:CAEITE>2.0.CO;2.

Begin, Z.B., Stein, M., Katz, A., Machlus, M., Rosenfeld, A., Buchbinder, B., Bartov, Y., 2004. Southward migration of rain tracks during the last glacial, revealed by salinity gradient in Lake Lisan (Dead Sea rift). Quat. Sci. Rev. 23 (14), 1627–1636. https://doi.org/10.1016/j.quascirev.2004.01.002.

Belmaker, R., Lazar, B., Beer, J., Christl, M., Tepelyakov, N., Stein, M., 2013. ^{10}Be dating of Neogene halite. Geochim. Cosmochim. Acta 122, 418–429. https://doi.org/10.1016/j.gca.2013.08.033.

Eggenkamp, H.G.M., 2015. Comment on "Stable isotope fractionation of chlorine during the precipitation of single chloride minerals" by Luo, C., Xiao, K., Wen, H., Ma, H., Ma, Y., Zhang, Y., Zhang, Y. and He, M. [Applied Geochemistry 47 (2014) 141–149]. Appl. Geochem. 54, 111–116.

Eggenkamp, H.G.M., Kreulen, R., Koster Van Groos, A.F., 1995. Chlorine stable isotope fractionation in evaporites. Geochim. Cosmochim. Acta 59 (24), 5169–5175. https://doi.org/10.1016/0016-7037(95)00353-3.

Eggenkamp, H.G.M., Bonifacie, M., Ader, M., Agrinier, P., 2016. Experimental determination of stable chlorine and bromine isotope fractionation during precipitation of salt from a saturated solution. Chem. Geol. 433, 46–56. https://doi.org/10.1016/j.chemgeo.2016.04.009.

Frumkin, A., 1996. Determining the exposure age of a karst landscape. Quat. Res. 46 (2), 99–106. https://doi.org/10.1006/qres.1996.0050.

Frumkin, A., Ford, D.C., 1995. Rapid entrenchment of stream profiles in the salt caves of Mount Sedom, Israel. Earth Surf. Process. Landf. 20, 139–152. https://doi.org/10.1002/esp.3290200205.

García-Veigas, J., Rosell, L., Zak, I., Playà, E., Ayora, C., Starinsky, A., 2009. Evidence of potash salt formation in the Pliocene Sedom lagoon (Dead Sea Rift, Israel). Chem. Geol. 265 (3), 499–511. https://doi.org/10.1016/j.chemgeo.2009.05.013.

Gavrieli, I., 1997. Halite deposition from the Dead Sea: 1960–1993. In: Oxford Monographs on Geology and Geophysics, vol. 36, pp. 161–170.

Gavrieli, I., Starinsky, A., Bein, A., 1989. The solubility of halite as a function of temperature in the highly saline Dead Sea brine system. Limnol. Oceanogr. 34 (7), 1224–1234. https://doi.org/10.4319/lo.1989.34.7.1224.

Gavrieli, I., Stein, M., 2006. On the origin and fate of the brines in the Dead Sea basin. Spec. Pap., Geol. Soc. Am. 401, 183–194. https://doi.org/10.1130/2006.2401(12).

Golan, R., Gavrieli, I., Ganor, J., Lazar, B., 2016. Controls on the pH of hyper-saline lakes – a lesson from the Dead Sea. Earth Planet. Sci. Lett. 434, 289–297. https://doi.org/10.1016/j.epsl.2015.11.022.

Hall, J.K., 1996. Digital topography and bathymetry of the area of the Dead Sea depression. Tectonophysics 266 (1–4), 177–185. https://doi.org/10.1016/S0040-1951(96)00189-8.

Hsü, K.J., Ryan, W.B.F., Cita, M.B., 1973. Late Miocene desiccation of the Mediterranean. Nature 242 (5395), 240–244.

Katz, A., Kolodny, Y., Nissenbaum, A., 1977. The geochemical evolution of the Pleistocene Lake Lisan–Dead Sea system. Geochim. Cosmochim. Acta 41 (11), 1609–1611. https://doi.org/10.1016/0016-7037(77)90172-7.

Katz, A., Starinsky, A., 2009. Geochemical history of the Dead Sea. Aquat. Geochem. 15 (1–2), 159–194.

Kiro, Y., Goldstein, S.L., Lazar, B., Stein, M., 2016. Environmental implications of salt facies in the Dead Sea. Geol. Soc. Am. Bull. 128 (5–6), 824–841. https://doi.org/10.1130/B31357.1.

Kiro, Y., Goldstein, S.L., García-Veigas, J., Levy, E., Kushnir, Y., Stein, M., Lazar, B., 2017. Relationships between lake-level changes and water and salt budgets in the Dead Sea during extreme aridities in the Eastern Mediterranean. Earth Planet. Sci. Lett. 464, 211–226. https://doi.org/10.1016/j.epsl.2017.01.043.

Kitagawa, H., Stein, M., Goldstein, S.L., Nakamura, T., Lazar, B., 2017. Radiocarbon chronology of the DSDDP core at the deepest floor of the Dead Sea. Radiocarbon 59 (2), 383–394. https://doi.org/10.1017/RDC.2016.120.

Lazar, B., Sivan, O., Yechieli, Y., Levy, E.J., Antler, G., Gavrieli, I., Stein, M., 2014. Long-term freshening of the Dead Sea brine revealed by porewater Cl^- and $\delta^{18}O$ in ICDP Dead Sea deep-drill. Earth Planet. Sci. Lett. 400, 94–101. https://doi.org/10.1016/j.epsl.2014.03.019.

Lensky, N.G., Dvorkin, Y., Lyakhovsky, V., Gertman, I., Gavrieli, I., 2005. Water, salt, and energy balances of the Dead Sea. Water Resour. Res. 41 (12). https://doi.org/10.1029/2005WR004084.

Levy, E.J., Stein, M., Lazar, B., Gavrieli, I., Yechieli, Y., Sivan, O., 2017. Pore fluids in Dead Sea sediment core reveal linear response of lake chemistry to global climate changes. Geology 45 (4), 315–318. https://doi.org/10.1130/G38685.1.

Lüthi, D., Le Floch, M., Bereiter, B., Blunier, T., Barnola, J.M., Siegenthaler, U., Raynaud, D., Jouzel, J., Fischer, H., Kawamura, K., Stocker, T.F., 2008. High-resolution carbon dioxide concentration record 650,000–800,000 years before present. Nature 453 (7193), 379. https://doi.org/10.1038/nature06949.

Luo, C., Xiao, Y., Ma, H., Ma, Y., Zhang, Y., He, M., 2012. Stable isotope fractionation of chlorine during evaporation of brine from a saline lake. Chin. Sci. Bull. 57 (15), 1833–1843.

Luo, C., Xiao, Y., Wen, H., Ma, H., Ma, Y., Zhang, Y., Zhang, Y., He, M., 2014. Stable isotope fractionation of chlorine during the precipitation of single chloride minerals. Appl. Geochem. 47, 141–149. https://doi.org/10.1016/j.apgeochem.2014.06.005.

Luo, C.G., Xiao, Y.K., Wen, H.J., Ma, H.Z., Ma, Y.Q., Zhang, Y.L., He, M.Y., 2015. Reply to the comment on the paper "Stable isotope fractionation of chlorine during the precipitation of single chloride minerals". Appl. Geochem. 54, 117–118.

Matmon, A., Fink, D., Davis, M., Niedermann, S., Rood, D., Frumkin, A., 2014. Unraveling rift margin evolution and escarpment development ages along the Dead Sea fault using cosmogenic burial ages. Quat. Res. 82 (1), 281–295. https://doi.org/10.1016/j.yqres.2014.04.008.

Neugebauer, I., Brauer, A., Schwab, M.J., Waldmann, N.D., Enzel, Y., Kitagawa, H., Torfstein, A., Frank, U., Dulski, P., Agnon, A., Ariztegui, D., 2014. Lithology of the long sediment record recovered by the ICDP Dead Sea Deep Drilling Project (DSDDP). Quat. Sci. Rev. 102, 149–165. https://doi.org/10.1016/j.quascirev.2014.08.013.

Neugebauer, I., Schwab, M.J., Waldmann, N.D., Tjallingii, R., Frank, U., Hadzhiivanova, E., Naumann, R., Taha, N., Agnon, A., Enzel, Y., Brauer, A., 2016. Hydroclimatic variability in the Levant during the early last glacial ($\sim$117–75 ka) derived from micro-facies analyses of deep Dead Sea sediments. Clim. Past 12 (1), 75–90. https://doi.org/10.5914/cp-12-75-2016.

Palchan, D., Neugebauer, I., Amitai, Y., Waldmann, N.D., Schwab, M.J., Dulski, P., Brauer, A., Stein, M., Erel, Y., Enzel, Y., 2017. North Atlantic controlled depositional cycles in MIS 5e layered sediments from the deep Dead Sea basin. Quat. Res. 87 (1), 168–179. https://doi.org/10.1017/qua.2016.10.

Parkhurst, D.L., Appelo, C.A.J., 1999. User's guide to PHREEQC (Version 2): a computer program for speciation, batch-reaction, one-dimensional transport, and inverse geochemical calculations.

Pe'eri, S., Zebker, H.A., Ben-Avraham, Z., Frumkin, A., Hall, J.K., 2004. Spatially-resolved uplift rate of the Mount Sedom (Dead Sea) salt diapir from InSAR observations. Isr. J. Earth-Sci. 53 (2).

Pitzer, K.S., 1973. Thermodynamics of electrolytes, I: theoretical basis and general equations. J. Phys. Chem. 77 (2), 268–277.

Shouakar-Stash, O., Frape, S.K., Drimmie, R.J., 2005. Determination of inorganic chlorine stable isotopes by continuous flow isotope ratio mass spectrometry. Rapid Commun. Mass Spectrom. 19, 121–127. https://doi.org/10.1002/rcm.1762.

Sirota, I., Enzel, Y., Lensky, N.G., 2017. Temperature seasonality control on modern halite layers in the Dead Sea: in situ observations. Geol. Soc. Am. Bull. https://doi.org/10.1130/B31661-1.

Starinsky, A., 1974. Relationship Between Ca-Chloride Brines and Sedimentary Rocks in Israel. Doctoral Dissertation.

Stein, M., 2001. The sedimentary and geochemical record of Neogene–Quaternary water bodies in the Dead Sea basin-inferences for the regional paleoclimatic history. J. Paleolimnol. 26 (3), 271–282.

Stein, M., 2014. The evolution of Neogene–Quaternary water-bodies in the Dead Sea rift valley. In: Dead Sea Transform Fault System: Reviews. Springer, Netherlands, pp. 279–316.

Stein, M., Torfstein, A., Gavrieli, I., Yechieli, Y., 2010. Abrupt aridities and salt deposition in the post-glacial Dead Sea and their North Atlantic connection. Quat. Sci. Rev. 29, 567–575. https://doi.org/10.1016/j.quascirev.2009.10.015.

Stein, M., Ben-Avraham, Z., Goldstein, S.L., 2011. Dead Sea deep cores: a window into past climate and seismicity. Eos (Trans. Am. Geophys. Union) 92, 453–454. https://doi.org/10.1029/2011EO490001.

Steinhorn, I., 1983. In situ salt precipitation at the Dead Sea. Limnol. Oceanogr. 28 (3), 580–583.

Stiller, M., Nissenbaum, A., Kaufmann, R.S., Long, A., 1998. Cl-37 in the Dead Sea system-preliminary results. Appl. Geochem. 13 (8), 953–960. https://doi.org/10.1016/S0883-2927(98)00017-1.

Torfstein, A., Goldstein, S.L., Kushnir, Y., Enzel, Y., Haug, G., Stein, M., 2015. Dead Sea drawdown and monsoonal impacts in the Levant during the last interglacial. Earth Planet. Sci. Lett. 412, 235–244. https://doi.org/10.1016/j.epsl.2014.12.013.

Vroman, J., 1950. The movement and solution of salt bodies as applied to Mount Sdom. Isr. Explor. J. 1, 185–193.

Weinberger, R., Begin, Z.B., Waldmann, N., Gardosh, M., Baer, G., Frumkin, A., Wdowinski, S., 2006. Quaternary rise of the Sedom diapir, Dead Sea basin. Spec. Pap., Geol. Soc. Am. 401, 33–51. https://doi.org/10.1130/2006.2401(03).

Weinberger, R., Bar-Matthews, M., Levi, T., Begin, Z.B., 2007. Late-Pleistocene rise of the Sedom diapir on the backdrop of water-level fluctuations of Lake Lisan, Dead Sea basin. Quat. Int. 175 (1), 53–61. https://doi.org/10.1016/j.quaint.2007.03.007.

Zak, I., 1967. The Geology of Mt. Sedom. Ph.D. Thesis. The Hebrew University, Jerusalem (in Hebrew with English abstract).

Zilberman, T., Gavrieli, I., Yechieli, Y., Gertman, I., Katz, A., 2017. Constraints on evaporation and dilution of terminal, hypersaline lakes under negative water balance: the Dead Sea, Israel. Geochim. Cosmochim. Acta 217, 384–398. https://doi.org/10.1016/j.gca.2017.08.040.